HHS Public Access

Author manuscript

Stroke. Author manuscript; available in PMC 2016 June 08.

Published in final edited form as:

Stroke. 2012 February ; 43(2): 524–531. doi:10.1161/STROKEAHA.111.635672.

PLASMALEMMA PERMEABILITY AND NECROTIC CELL DEATH PHENOTYPES AFTER INTRACEREBRAL HEMORRHAGE IN MICE

Xiaoxia Zhu, MD[1,2,5,*], **Luyang Tao, MD, PhD**[1,2,6,*], **Emiri Tejima-Mandeville, PhD**[1,3,4], **Jianhua Qiu, MD, PhD**[1,2], **Juyeon Park, BA**[1,2], **Kent Garber**[1,2], **Maria Ericsson, BS**[7], **Eng H. Lo, PhD**[1,3,4], and **Michael J. Whalen, MD**[1,2]

[1]Neuroscience Center, Massachusetts General Hospital, Charlestown, Massachusetts, 02129

[2]Department of Pediatrics, Massachusetts General Hospital, Charlestown, Massachusetts, 02129

[3]Department of Radiology, Massachusetts General Hospital, Charlestown, Massachusetts, 02129

[4]Department of Neurology, Massachusetts General Hospital, Charlestown, Massachusetts, 02129

[5]Department of Rheumatology, Huashan Hospital, Fudan University, Shanghai, China, 200040

[6]Department of forensic medicine, Soochow University, Suzhou 215123, China

[7]Harvard Medical School Electron Microscopy Facility, 220 Longwood Avenue, Boston, MA 02115

Abstract

Background and purpose—Traumatic and ischemic brain injury induce plasmalemma permeability and necrosis however no studies have examined these aspects of cellular injury in intracerebral hemorrhage (ICH) models.

Methods—In vivo propidium iodide (PI) and YOYO-1 were used to assess plasmalemma damage after collagenase-induced ICH in mice. Ex vivo aspartylglutamylvalylaspartic acid (DEVD), TUNEL, and electron microscopy were used to assess the relationship between plasmalemma permeability and mode of cell death. Cell types vulnerable to plasmalemma damage were determined by immunohistochemistry.

Results—Plasmalemma permeability was first detected in the lesion at 1–3 h and peaked at 48–72 h. Neurons and IBA-1-positive cells with morphological features of monocytes were sensitive whereas resident microglia and astrocytes were resistant to plasmalemma permeability. PI+ cells colocalized with fluorescent labeled caspase substrates and TUNEL beginning at 3–6 h. At 48 h, greater than half of injured cells were PI+/DEVD− or PI+/TUNEL TUNEL− suggesting necrosis,

Address correspondence to: Michael J. Whalen, MD, Department of Pediatric Critical Care Medicine, Massachusetts General Hospital and Harvard Medical School, 149 13th Street, Charlestown, MA 02129. Phone: 617-724-4380; Fax: 617-724-4391; MWhalen@Partners.org.

*These authors contributed equally to the work.

The authors have no conflicts of interests or disclosures to report

and less than 5% were PI−/TUNEL+ or PI−/DEVD+. Electron microscopy confirmed ultrastructural features of necrosis at 24 h after ICH, HMGB1 was released from permeable cells, and mice deficient in RIPK3, a known necrosis trigger, had 50% less PI+ cells at 24 h. Permeable cells remained in brain for at least 24 h, with less than 10% spontaneous resealing.

Conclusion—Necrosis contributes to cell demise after ICH. Programmed necrosis and plasmalemma damage may represent novel therapeutic targets to prevent cell death or rescue injured cells after ICH.

Keywords

Intracerebral hemorrhage; inflammation; plasmalemma; apoptosis; necrosis; mice

Introduction

Experimental models of intracerebral hemorrhage (ICH) and brain specimens from humans with ICH show delayed progressive cell death in hemorrhagic brain[1–5]. Loss of plasmalemma integrity is a hallmark of cellular injury and death following renal and cerebral ischemia and traumatic brain injury (TBI)[6–9]. In experimental cerebral contusion, injured cells sustain plasmalemma damage early after injury and are degenerative by histochemical criteria, disappear from injured brain within several days, and have biochemical and ultrastructural features of necrosis[8]. In contrast, plasmalemma permeability after ischemic brain injury is delayed by several hours and peaks later than in cerebral contusion[6, 7]. Whether or not plasmalemma permeability is induced by intracerebral hemorrhage has not been previously reported. This is an important gap in the literature because plasma membrane permeability has been implicated as an initiating event in cell death as well as a trigger for the ensuing inflammatory response[10, 11].

Although numerous mechanisms of cell death including caspase-mediated apoptosis have been implicated in experimental ICH, surprisingly little study has been done to estimate the contribution of necrosis. One indirect way to assess necrosis is to interrogate plasmalemma function at the same time as caspase activity and DNA damage[6, 7, 9]. Early necrosis produces rapid loss of membrane integrity whereas membrane integrity is maintained until late stages of apoptotic cell death[6, 12, 13]. Thus, early necrosis might show plasmalemma damage with or without DNA damage, whereas early apoptosis is associated with DNA damage with plasmalemma integrity maintained. Cells with plasmalemma permeability and DNA damage may be late necrotic, late apoptotic, or a mixed cell death phenotype initiated by concomitant activation of necrotic and apoptotic mechanisms[8,9].

Acute ischemic and TBI induces plasmalemma permeability to PI through mechanisms that remain unknown[6–8]. We and others have used propidium iodide (PI) and the green fluorescent dye YOYO-1 iodide in vivo to label injured cells after ischemic and TBI[6–8]. These studies have demonstrated apoptotic-like (PI−/TUNEL+) and necrotic-like (PI+/TUNEL TUNEL−) cell death phenotypes. Here, we used in vivo PI and YOYO-1 to identify cells with plasmalemma permeability and follow their spatial and temporal course after collagenase-induced ICH in mice. Using ex vivo TUNEL and caspase histochemistry, and ultrastructural analysis of injured cells, we tested the hypothesis that plasmalemma

permeability is associated with markers of cell death and that a necrotic-like cell death phenotype is associated with ICH.

Methods

Collagenase-induced intracerebral hemorrhage in mice

All procedures and experimental protocols outlined below were approved by the MGH Institution for Animal Care and Use Committee, and complied with the NIH Guide for the Care and Use of Laboratory Animals. Male CD-1 mice ages 8–12 weeks weighing 25–35 g (Jackson Labs) were used for all studies except for comparisons between receptor interacting protein kinase 3 knock out (RIPK3 KO, backcrossed over 14 times into C57Bl/6) mice (a kind gift of Dr. Vishva Dixit, Genentech, San Francisco, Ca) and C57Bl/6 wild type mice (Supplemental Table 1). Mice were anesthetized with isoflurane/nitrous oxide/oxygen. A craniotomy was performed and a 32-gauge needle was lowered into the striatum (stereotactic coordinates from bregma: 1 mm anterior to 1mm posterior, 2 mm lateral, 3.5 mm depth). Type IV collagenase (0.03U/0.04μl; Sigma) or PBS vehicle was infused over 5 minutes. The needle was left in place for another 5 minutes then removed, the scalp sutured closed, and mice were recovered in room air. Blood-brain barrier damage was assessed at 24 h by injecting 5 ml/kg 2% Evans blue dye intravenously and examining frozen brain sections by fluorescence microscopy. Motor function was assessed using the wire grip test[14].

Preparation of brain tissue and detection of PI+ and YOYO-1+ cells

We detected cells with altered plasma membrane integrity using YOYO-1 and propidium iodide (PI) as previously described[8]. YOYO-1 (Molecular Probes; 1 ug/g in 150 μl phosphate-buffered saline [PBS]) is a cell membrane impermeant cyanine nucleic acid stain with excitation-emission maxima at 491/509 nm that has been used to document plasmalemma permeability and resealing in vivo[8]. YOYO-1 was administered intravenously. In experiments designed to assess for spontaneous plasmalemma resealing, propidium iodide (PI; 1 ug/g mouse in 150 μL PBS; Sigma) was administered IV as well. For all other experiments, PI was administered by the intraperitoneal (IP) route. Mice were deeply anesthetized with isoflurane and killed at various times after ICH. Brains were removed and frozen in liquid nitrogen vapor and stored at −80°C. Brains sections (12 μm thick) were cut on a cryostat 150 to 200 μm apart from anterior to posterior lesion, placed on poly-L-lysine-coated glass slides and stored at −80°C. Alternatively, for IBA-1 immunohistochemistry, mice were transcardially perfused with 4% paraformaldehyde and brains post-fixed in 4% paraformaldehyde over night, cryoprotected in 30% sucrose, and cut on a cryostat as above. Brain sections were photographed and analyzed by fluorescence microscopy (Nikon Eclipse T300 fluorescence microscope, Tokyo, Japan) using excitation and emission wavelengths for PI 568 and 585 nm and YOYO-1 490 nm and 520 nm, respectively. Operational definitions of cell death phenotypes were based on criteria from previous studies[6–9, 14]. The pure necrosis phenotype is defined as PI+/TUNEL TUNEL−; pure apoptosis is defined as PI−/TUNEL+; and the mixed cell death phenotype is defined as PI+/TUNEL+. To show that PI and YOYO-1 label nucleated cells in the ICH model, some brain sections were counterstained with Hoechst 33342 (Thermo Scientific, Rockford, IL) (1:1000) for 15 s.

Detection of in situ caspase activity and TUNEL

Carboxyfluorescein analogs of aspartylglutamylvalylaspartic acid fluoromethyl ketone (FAM-DEVD-FMK, caspase-3 inhibitor), leucylglutamylthreonylaspartic fluoromethyl ketone (FAM-LETD-FMK, caspase-8 inhibitor), and leucylglutamylhistidylaspartic acid fluoromethyl ketone (FAM-LEHD-FMK, caspase-9 inhibitor) were reconstituted according to the instructions from the manufacturer (BioCarta), diluted 1:75,000 in phosphate buffered saline (pH 7.2), and reacted for 60 seconds with unfixed, frozen brain sections at room temperature. TUNEL was performed as previously described[8].

Immunohistochemistry

For immunohistochemical detection of HMGB1 or glial cell types labeled with PI or YOYO-1, paraformaldehyde fixed/perfused brain sections were washed in PBS and blocked in 2% normal goat serum and reacted with anti-mouse GFAP conjugated to Cy3 (1:300, Sigma), rabbit anti-mouse IBA-1 (1:200, Wako), rabbit anti-HMGB1 (Abcam, Cambridge, MA) or anti-NeuN (1:300, Chemicon) conjugated to Cy3 (Amersham Biosciences). Anti-rabbit FITC conjugated secondary antibodies (1:300, Jackson Immunological labs) were used to detect IBA-1. Sections were washed and mounted in 100% ethanol, coverslipped and photographed using fluorescence microscopy.

Quantitation of cell count data

YOYO-1+ and PI+ cells in CD1 mice and RIPK3 KO and C57Bl/6 WT mice were counted in x200 fields (1,100 μm×1,100 μm) randomly chosen from four to five brain sections separated by at least 150 μm, located within the lesion produced by ICH. Fields from the periphery (n = 8) and core (n = 8) of the hemorrhagic lesion (defined anatomically as the inner half of the lesion) were counted from the brain sections analyzed. For PI/TUNEL and PI/caspase substrate cell counts, 6 fields per mouse were assessed from equal numbers of core and peripheral regions of the ICH, or from 6 peripheral or 6 core regions for studies of core vs. peripheral hemorrhagic regions. For quantitation of spontaneous resealing, all YOYO-1+ cells and YOYO-1+/PI−cells were counted in 8–10 ×200 fields randomly chosen in peripheral and core brain regions among 5–6 brain sections per mouse. Resealed cells were defined as YOYO-1+/PI− and non-resealed cells as YOYO-1+/PI+. Data for each mouse were the averages of the cell counts in the x200 fields.

Electron microscopy

Electron microscopy (EM) was performed as previously described with minor modifications[8]. Mice were deeply anesthetized and transcardially perfused with 2% paraformaldehyde/2% glutaraldehyde (EM grade, Sigma) in PBS, pH 7.4. Brains were post-fixed overnight and cryoprotected in sucrose and 4 mm brain sections were cut from the ICH region. For electron microscopy, brain tissue was cut on a microtome and sections were post fixed with a mixture of 1% Osmium tetroxide + 1.5% potassium ferrocyanide (KFeCN6) for 30 minutes, washed in water and stained in 1% aqueous uranyl acetate for 30 minutes followed by dehydration in alcohol and then infiltrated and embedded in TAAB Epon (Marivac Canada). Ultrathin sections (60–80 nm) were cut on a Reichert Ultracut-S

microtome, stained with 0.2% lead citrate and examined in a Tecnai G^2 Spirit BioTWIN Transmission electron microscope. Images were taken with a 2k AMT CCD camera.

Statistical Analyses

Data are mean ± SEM. Cell count data were evaluated by analysis of variance (ANOVA) followed by Bonferroni's test. PI+ cells in RIPK3 KO and WT mice were analyzed by rank sum. Motor data were analyzed by repeated measures analysis of variance (RM ANOVA, group × time). For all comparisons, $p < 0.05$ was regarded as significant.

Results

Intrastriatal collagenase injection produced ICH in ipsilateral striatum within 1 h, with blood-brain barrier damage and motor deficits (Supplemental Figure 1). No injury was produced in contralateral hemispheres and injured cells (PI+, YOYO-1+, TUNEL+, DEVD +) were only detected in hemorrhagic brain regions in the ipsilateral hemisphere. Sham injury (injection of PBS instead of collagenase) produced no ICH lesion and only a few PI+ cells along the needle tract (data not shown).

Figure 1A shows representative photomicrographs of PI+ cells after collagenase-induced ICH. PI+ cells were detected as early as 1 h and peaked between 48–72 h (Figure 1B; $p < 0.001$ ANOVA for all time points). At early time points, PI+ cells were mainly distributed within the periphery of the hemorrhagic lesion but at 24–48 h many PI+ cells were also present in core regions. PI+ cells exhibited at least two general labeling patterns, with round, smooth nuclei consistent with necrotic-like morphology and condensed, fragmented nuclear labeling consistent with apoptosis[9], and all PI+ cells colocalized with Hoechst labeling, although not all Hoechst+ cells were PI+ (Figure 1B).

To determine identity of cell types sensitive to plasmalemma permeability we administered YOYO-1 intravenously after ICH and subjected frozen brain tissue sections to ex vivo immunohistochemistry. No YOYO-1+/IBA-1+ microglia (Figure 2A) or YOYO-1+/GFAP+ astrocytes (Figure 2B) were detected at 6 h after ICH, however YOYO-1+/NeuN+ neurons frequently were detected (Figure 2C). By 24 h, a few IBA-1+ microglia and a large number of spherical IBA-1+ cells that lacked the characteristic processes of brain microglia colocalized with YOYO-1 within hemorrhagic brain regions (Figure 2D). YOYO-1+/GFAP+ cells were not detected at 24 h and YOYO-1+/NeuN+ neurons were robustly detected. At 48 and 72 h, no GFAP+ cells had plasmalemma damage and almost all GFAP+ and IBA-1+ cells were strikingly localized around the outside the hemorrhagic lesion, a pattern that persisted for up to 14 d (Supplementary Figure 2). Thus, within the first 24–72 h, plasmalemma permeability was mainly detected in neurons, and IBA-1+ cells with morphological features of monocytes, within the hemorrhagic lesion, whereas microglia and astrocytes (which localized mainly around the periphery of the lesion) were resistant at all times examined.

To determine relationships between plasmalemma damage and putative modes of cell death we used in vivo PI labeling and ex vivo caspase substrate- or TUNEL-histochemistry. Figure 3 shows typical examples of PI+, caspase substrate+, and TUNEL+ cells and their

distribution at 48 h after ICH, the peak time of plasmalemma permeability. Fluorescent labeled DEVD-FMK detected activated caspases because positive staining was not observed using vehicle alone and was inhibited by pretreatment with non-labeled ZVAD, a pan-caspase inhibitor (not shown). At 6–48 h after ICH, PI+ cells often colocalized with caspase substrates (DEVD, LETD, and LEHD) or TUNEL (Figure 3A, LETD and LEHD not shown). At 24 h, PI/TUNEL cell count data in peripheral fields were PI+/TUNEL TUNEL−, 40 ± 8; PI−/TUNEL+ 7 ± 1; PI+/TUNEL+ 52 ± 7 cells/x200 field. At 48 h, PI+/DEVD− and PI+/TUNEL− cells accounted for over half of all PI+ cells (Figure 3B), whereas PI−/DEVD + and PI−/TUNEL+ cells were fewer than 5% each. At 48 h, PI/TUNEL cell count data were remarkably similar in peripheral (PI+/TUNEL TUNEL−, 59 ± 6; PI−/TUNEL+ 2 ± 0; PI+/TUNEL+ 42 ± 5 cells/x200 field) and core brain regions (PI+/TUNEL TUNEL−, 45 ± 3, PI−/TUNEL+, 2 ± 1, PI+/TUNEL+, 39 ± 4 cells/x200 field). At 24 and 48 h, a pure necrotic death phenotype (PI+/TUNEL TUNEL−) accounted for over 40 and 50%, respectively, of PI+ cells.

To confirm the presence of necrotic cell death we performed ultrastructural analyses of injured cells randomly selected from hemorrhagic brain at 24 h after ICH, biochemical analysis of HMGB1 release, and quantitation of PI+ cells at 24 h after ICH in RIPK3 KO vs. WT mice. Cells with morphological features of necrosis such as mitochondrial swelling, nuclear membrane disintegration, and characteristic nuclear karyorrhexis were observed, in addition to classical apoptotic bodies associated with apoptotic cell death (Figure 4 and apoptotic bodies not shown). HMGB1 release was robust in cells within the hemorrhagic zone, and HMGB1 was strikingly absent from almost all YOYO-1+ cells at 6 h (Supplemental Figure 3). At 24 h, no HMGB1 immunostaining was observed in the hemorrhage zone (not shown), and RIPK3 KO mice had over 50% reduction in PI+ cells in hemorrhagic peripheral and core regions (Figure 5).

To assess survival time of injured cells, and whether permeable cells may repair their membrane damage after ICH, we administered YOYO-1 at 24 or 48 h, followed by PI at 48 or 72 h, respectively, to label YOYO-1+ cells with persistent plasmalemma damage. Brain sections were analyzed for the presence of YOYO-1+ and PI+ cells. Most YOYO-1+ cells labeled at 24 h (94.4 ± 2.0 %) or 48 h (98.7 ± 0.7%) also co-labeled with PI at 48 or 72 h, respectively, indicating only a minor prevalence of spontaneous membrane resealing (Figure 6 and 48–72 h data not shown).

Discussion

To our knowledge this is the first description of plasmalemma permeability and necrotic cell death in an ICH model. As previously reported in adult stroke and brain trauma models[6–8], in vivo PI and YOYO-1 labeling appears to be specific for cells with loss of membrane integrity in ICH, as PI co-localized with only a subset of Hoechst+ cells, and PI labeling was not observed in uninjured hemispheres or in PBS-injected mice (except along the needle tract). Moreover, PI labeling followed a discrete temporal course that peaked at 48–72 h, and plasmalemma damage occurred in specific cell types (neurons and IBA1+ cells but not astrocytes) within the first 24–72 h. PI and YOYO-1 labeling only occurred in nucleated cells as demonstrated by Hoechst colabeling, ruling out artifactual labeling of erythrocytes

which lack a nucleus. These data suggest the validity of using in vivo PI and YOYO-1 to detect plasmalemma permeability in injured parenchymal cells as we and others have reported in other acute brain and renal injury models[6–9].

The time course of plasmalemma damage in ICH is similar to that reported in murine ischemic stroke in which PI+ cells were first observed approximately 6 h after middle cerebral artery occlusion and reperfusion[6]. It is unlikely that direct membrane disruption by collagenase is a primary mechanism of plasmalemma damage because the peak of PI+ cells would be predicted to occur much earlier in this case. Robust blood brain barrier damage is present from 1 to at least 48 h in our collagenase ICH model (24 h data shown in Supplementary Figure 1). Thus, PI (640 Da) can easily gain entry to parenchymal cells via the damaged BBB. The time course of plasmalemma permeability after experimental cerebral contusion, in which ICH contributes to tissue damage, was considerably faster with PI+ cells peaking at 1–6 h after controlled cortical impact (CCI) in vulnerable brain regions[8]. Because we did not assess 4–6 d, it is possible that plasmalemma permeability might peak later than 72 h after ICH. The differences in kinetics of plasmalemma damage in cerebral contusion (early) and collagenase-induced ICH (delayed) are not explained by delayed bleeding in ICH (collagenase injection produces a large hematoma by 1 h) or by differences in amounts of fluorophore administration in CCI[8] and the current study.

Cell types vulnerable to plasmalemma damage within the first 24 h were similar to those reported in neonatal and adult ischemic stroke models[6, 15] and in TBI[8]. Neurons and rounded IBA1+ cells lacking processes were most vulnerable. The lack of plasmalemma damage in glial cells (almost all of which were detected outside the ICH lesion from 6 to 72 h) and the low numbers of PI+ cells remaining at 7 d suggests that astrocytes and most microglia are relatively resistant to plasmalemma damage after collagenase ICH. Astrocyte resistance to plasmalemma damage was also reported in neonatal rat hypoxic-ischemic brain injury[16], and in focal stroke in adult mice in which astrocytes exhibited delayed loss of plasmalemma and mitochondrial integrity and reduced ultrastructural damage compared to neurons[17]. Neurons are highly vulnerable to early plasmalemma damage after stroke and TBI[6–8] and ICH as suggested by the current study.

We found robust plasmalemma damage in IBA1+ cells within the ICH lesion at 24 h. IBA-1+ cells could represent activated microglia with loss of processes or blood-borne monocytes. Making this distinction is an important goal of future studies, because blood borne monocytes play a protective role in preserving neurons and improving functional outcome after spinal cord and ischemic retinal injury, presumably by producing a milieu that limits the overall inflammatory response and subsequent neuronal death[18,19]. Monocytes and microglia may facilitate resolution of ICH by phagocytosing erythrocytes and their toxic intracellular constituents which drive neurodegeneration[20]. On the other hand, inhibition of microglial transmigration and function reduced brain edema and inflammation early after experimental ICH[21]. Thus, monocytes and microglia may exert beneficial or detrimental effects on outcome after ICH depending in part on timing after injury.

In the majority of injured cells, plasmalemma damage occurred before detectable activation of caspases and DNA damage (TUNEL), suggesting a significant contribution of necrosis to

cell death after ICH[2]. TUNEL and caspase substrate analyses alone cannot be used to rule in or out a specific cell death mode in CNS injury because TUNEL may label necrotic as well as apoptotic cells[9] and caspases may be activated during necrotic cell death[7, 13]. The temporal sequence of plasmalemma damage followed by DNA damage and/or caspase activation is suggestive of necrosis in collagenase-induced ICH. This tentative conclusion is supported by ultrastructural analyses of a limited number of cells showing patterns of chromatin condensation, dissolution of nuclear and plasma membranes, and mitochondrial swelling characteristic of necrosis (Figure 4). We and others have demonstrated heterogeneous cell death phenotypes, including necrosis, in acute CNS injury paradigms using in vivo PI labeling[7, 8, 14] and necrosis has also been reported in human brain samples obtained at autopsy from patients with ICH[22].

High mobility group box protein-1 (HMGB1) is a non-histone nuclear protein and prototype member of the alarmin family of damage-associated molecular proteins (DAMPs). HMGB1 is released from dead or dying cells when membrane integrity is compromised and interacts with specific receptors on immune cells, as well as with other DAMPs such as LPS, DNA, and cytokines, to induce an inflammatory response[23]. Thus, HMGB1 released from necrotic cells drives immune responses and promotes inflammation. In the current study, HMGB1 release was associated with loss of plasmalemma integrity in YOYO-1+ cells at 6 h after ICH. Because HMGB1 release is associated with necrosis and subsequent inflammation after ischemic stroke[24,25], its release from YOYO-1+ cells in hemorrhagic brain suggests that HMGB1 may link necrotic cell death with the ensuing inflammatory response after ICH.

Using YOYO-1 pulse labeling we found that over 90% of YOYO-1+ cells labeled at 24 or 48 h remained permeable to PI for at least 24 h, suggesting limited spontaneous membrane repair. In contrast, membrane permeability in injured neurons may be reversible in mild fluid percussion and more severe controlled cortical impact TBI models[8, 26]. The current data suggest that plasmalemma damage may portend fatal outcome after ICH. This possibility is also supported by the observation that a significant percentage of PI+ cells co-labeled with TUNEL and activated caspases, few PI+ cells were detected in hemorrhagic brain at 7 d (Figure 2), and by prior studies showing significant neuronal loss after ICH in rodents[27].

Our data suggest at least a 72 h window for rescue of significant numbers of PI+ cells after ICH, similar to that reported in CCI[8]. Necroptosis, a form of programmed necrosis mediated by receptor interacting kinase-1 (RIPK1)[28], is implicated in experimental stroke[28] and TBI[14] and in hemin-induced cell death in vitro[29]. Thus, necrostatins (specific inhibitors of RIPK1)[30] may have utility in preventing ICH-induced cell death. In the current study, RIPK3 KO mice had approximately 50% reduction in PI+ cells at 24 h compared to wild type, providing powerful proof of principle that plasmalemma permeability can be manipulated and that RIPK3 could mediate programmed necrosis (necroptosis) after ICH[31].

Other mechanisms of collagenase induced ICH that may lead to plasmalemma damage include hemoglobin- and iron-induced oxidative stress which may directly induce membrane damage and permeability[32]. Interestingly, hemoglobin induced cell death in primary rat cortical neurons involved caspase activation, but membrane damage and cell death were

inhibited by an anti-oxidant and not by caspase inhibitors[33]. These data lend support to the idea that necrosis and caspase mechanisms each contribute to ICH-induced cell death. Our findings also suggest that pharmacological membrane resealing may be an effective strategy to rescue injured cells or prevent bystander injury from release of damage associated molecular pathogens from permeabilized cells[34, 11]. Intracerebroventricular administration of Poloxamer P188, a prototype membrane resealing agent, reduced acute cell death after ICH in rats, but membrane resealing by P188 was not reported in that study[35]. Data from the current study provide a framework for novel therapeutic strategies to limit cell death and improve outcome after ICH in patients, for whom no specific therapy is currently available.

Supplementary Material

Refer to Web version on PubMed Central for supplementary material.

Acknowledgments

Support: China Natural Science Foundation (30571909 and 30872666, LT), R37-NS37074, P01-NS55104 (EHL), and RO1NS061255, RO1NS064545 (MJW)

References

1. Nguyen AP, Huynh HD, Sjovold SB, Colbourne F. Progressive brain damage and alterations in dendritic arborization after collagenase-induced intracerebral hemorrhage in rats. Curr Neurovasc Res. 2008; 5:171–177. [PubMed: 18691074]
2. Matsushita K, Meng W, Wang X, Asahi M, Asahi K, Moskowitz MA, et al. Evidence for apoptosis after intercerebral hemorrhage in rat striatum. J Cereb Blood Flow Metab. 2000; 20:396–404. [PubMed: 10698078]
3. Grossetete M, Rosenberg GA. Matrix metalloproteinase inhibition facilitates cell death in intracerebral hemorrhage in mouse. J Cereb Blood Flow Metab. 2008; 28:752–763. [PubMed: 17971790]
4. Wang J, Tsirka SE. Neuroprotection by inhibition of matrix metalloproteinases in a mouse model of intracerebral haemorrhage. Brain. 2005; 128:1622–1633. [PubMed: 15800021]
5. Qureshi AI, Suri MF, Ostrow PT, Kim SH, Ali Z, Shatla AA, et al. Apoptosis as a form of cell death in intracerebral hemorrhage. Neurosurgery. 2003; 52:1041–1047. discussion 1047–1048. [PubMed: 12699545]
6. Unal Cevik I, Dalkara T. Intravenously administered propidium iodide labels necrotic cells in the intact mouse brain after injury. Cell Death Differ. 2003; 10:928–929. [PubMed: 12868000]
7. Unal-Cevik I, Kilinc M, Can A, Gursoy-Ozdemir Y, Dalkara T. Apoptotic and necrotic death mechanisms are concomitantly activated in the same cell after cerebral ischemia. Stroke. 2004; 35:2189–2194. [PubMed: 15256676]
8. Whalen MJ, Dalkara T, You Z, Qiu J, Bermpohl D, Mehta N, et al. Acute plasmalemma permeability and protracted clearance of injured cells after controlled cortical impact in mice. J Cereb Blood Flow Metab. 2008; 28:490–505. [PubMed: 17713463]
9. Kelly KJ, Sandoval RM, Dunn KW, Molitoris BA, Dagher PC. A novel method to determine specificity and sensitivity of the TUNEL reaction in the quantitation of apoptosis. Am J Physiol Cell Physiol. 2003; 284:C1309–C1318. [PubMed: 12676658]
10. Serbest G, Horwitz J, Jost M, Barbee K. Mechanisms of cell death and neuroprotection by poloxamer P188 after mechanical trauma. FASEB. 2006; 20:308–310.
11. Kono H, Rock K. How dying cells alert the immune system to danger. Nat Rev Immunol. 2008; 8:279–289. [PubMed: 18340345]

12. Hong J, Lin T, Yang J, Hsu Y, Wu J. Dynamics of Nontypical Apoptotic MorphologicalChanges Visualized by Green Fluorescent Protein in Living Cells with Infectious Pancreatic Necrosis Virus Infection. J Virol. 1999; 73:5056–5063. [PubMed: 10233968]
13. Formigli L, Papucci L, Tani A, Schiavone N, Tempestini A, Orlandini GE, et al. Aponecrosis: Morphological and biochemical exploration of a syncretic process of cell death sharing apoptosis and necrosis. J Cell Physiol. 2000; 182:41–49. [PubMed: 10567915]
14. You Z, Savitz SI, Yang J, Degterev A, Yuan J, Cuny GD, et al. Necrostatin-1 reduces histopathology and improves functional outcome after controlled cortical impact in mice. J Cereb Blood Flow Metab. 2008; 28:1564–1573. [PubMed: 18493258]
15. Northington FJ, Ferriero DM, Graham EM, Traystman RJ, Martin LJ. Early neurodegeneration after hypoxia-ischemia in neonatal rat is necrosis while delayed neuronal death is apoptosis. Neurobiol Dis. 2001; 8:207–219. [PubMed: 11300718]
16. Carloni S, Carnevali A, Cimino M, Balduini W. Extended role of necrotic cell death after hypoxia-ischemia-induced neurodegeneration in the neonatal rat. Neurobiol Dis. 2007; 27:354–361. [PubMed: 17681771]
17. Gurer G, Gursoy-Ozdemir Y, Erdemli E, Can A, Dalkara T. Astrocytes are more resistant to focal cerebral ischemia than neurons and die by a delayed necrosis. Brain Pathol. 2009; 19:630–641. [PubMed: 18947334]
18. London A, Itskovich E, Benhar I, Kalchenko V, Mack M, Jung S, et al. Neuroprotection and progenitor cell renewal in the injured adult murine retina requires healing monocyte-derived macrophages. J Exp Med. 2011; 208:23–29. [PubMed: 21220455]
19. Kigerl KA, Gensel JC, Ankeny DP, Alexander JK, Donnelly DJ, Popovich PG. Identification of two distinct macrophage subsets with divergent effects causing either neurotoxicity or regeneration in the injured mouse spinal cord. J Neurosci. 2009; 29:13435–13444. [PubMed: 19864556]
20. Zhao X, Grotta J, Gonzales N, Aronowski J. Hematoma resolution as a therapeutic target: The role of microglia/macrophages. Stroke. 2009; 40:S92–S94. [PubMed: 19064796]
21. Ma Q, Manaenko A, Khatibi NH, Chen W, Zhang JH, Tang J. Vascular adhesion protein-1 inhibition provides antiinflammatory protection after an intracerebral hemorrhagic stroke in mice. J Cereb Blood Flow Metab. 2011; 31:881–893. [PubMed: 20877383]
22. Li H, Wang SR, Wang LK, Chen XF, Zhao CJ, Duan S, et al. Perihematomal pathological changes in neurons and astrocytes following acute cerebral hemorrhage. Int J Neurosci. 2010; 120:683–690. [PubMed: 20942581]
23. Pisetsky DS, Gauley J, Ullal AJ. HMGB1 and Microparticles as Mediators of the Immune Response to Cell Death. Antioxid Redox Signal. 2011; 15:2209–2219. [PubMed: 21194388]
24. Hayakawa K, Qiu J, Lo EH. Biphasic actions of HMGB1 signaling in inflammation and recovery after stroke. Ann N Y Acad Sci. 2010; 1207:50–57. [PubMed: 20955426]
25. Qiu J, Xu J, Zheng Y, Wei Y, Zhu X, Lo EH, et al. High mobility group box-1 promotes metalloproteinase-9 upregulation through toll like receptor 4 after cerebral ischemia. Stroke. 2010; 41:2077–2082. [PubMed: 20671243]
26. Farkas O, Lifshitz J, Povlishock JT. Mechanoporation induced by diffuse traumatic brain injury: An irreversible or reversible response to injury? J Neurosci. 2006; 26:3130–3140. [PubMed: 16554464]
27. Felberg RA, Grotta JC, Shirzadi AL, Strong R, Narayana P, Hill-Felberg SJ, et al. Cell death in experimental intracerebral hemorrhage: The "Black hole" Model of hemorrhagic damage. Ann Neurol. 2002; 51:517–524. [PubMed: 11921058]
28. Degterev A, Huang Z, Boyce M, Li Y, Jagtap P, Mizushima N, et al. Chemical inhibitor of nonapoptotic cell death with therapeutic potential for ischemic brain injury. Nat Chem Biol. 2005; 1:112–119. [PubMed: 16408008]
29. Laird MD, Wakade C, Alleyne CH Jr, Dhandapani KM. Hemin-induced necroptosis involves glutathione depletion in mouse astrocytes. Free Radic Biol Med. 2008; 45:1103–1114. [PubMed: 18706498]
30. Degterev A, Hitomi J, Germscheid M, Ch'en IL, Korkina O, Teng X, et al. Identification of rip1 kinase as a specific cellular target of necrostatins. Nat Chem Biol. 2008; 4:313–321. [PubMed: 18408713]

31. Zhang DW, Shao J, Lin J, Zhang N, Lu BJ, Lin SC, et al. RIP3, an energy metabolism regulator that switches TNF-induced cell death from apoptosis to necrosis. Science. 2009; 325:332–336. [PubMed: 19498109]

32. Balla J, Jacob HS, Balla G, Nath K, Eaton JW, Vercellotti GM. Endothelial cell heme uptake from heme proteins: Induction of sensitization and desensitization to oxidant damage. Proc Natl Acad Sci. 1993; 90:9285–9289. [PubMed: 8415693]

33. Wang X, Mori T, Lo EH. Hemoglobin-induced cytotoxicity in rat cerebral cortical neurons: Caspase activation and oxidative stress. Stroke. 2002; 33:1882–1888. [PubMed: 12105370]

34. Marks JD, Pan CY, Bushell T, Cromie W, Lee RC. Amphiphilic, tri-block copolymers provide potent membrane-targeted neuroprotection. Faseb J. 2001; 15:1107–1109. [PubMed: 11292683]

35. Cadichon SB, Le Hoang M, Wright DA, Curry DJ, Kang U, Frim DM. Neuroprotective effect of the surfactant poloxamer 188 in a model of intracranial hemorrhage in rats. J Neurosurg. 2007; 106:36–40. [PubMed: 17233310]

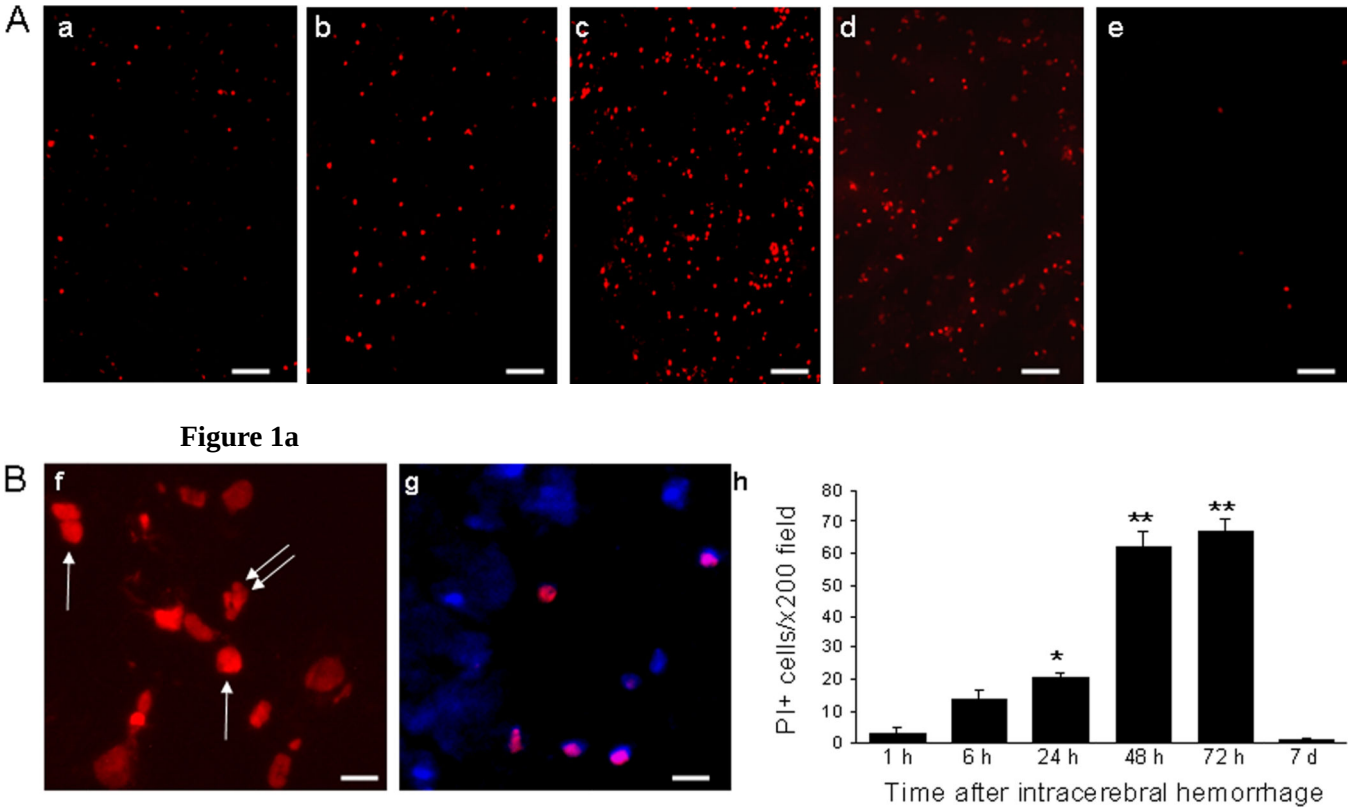

Figure 1a

Figure 1b

Figure 1.

Plasmalemma permeability detected by in vivo propidium iodide after intracerebral hemorrhage (ICH). (A) Representative photomicrographs of PI+ cells at (a) 6, (b) 24, (c) 48 h (d) 72 h, and (e) 7 d after intracerebral hemorrhage (ICH). (B) (f) Representative high magnification photomicrograph depicting PI+ cells with round, smooth nuclei (single arrows) suggestive of necrosis and others with lobulated nuclei (double arrows) suggestive of apoptosis. (g) Representative photomicrograph of a composite image made from merging images of PI+ and Hoechst+ cells from the same brain location. Note that not all Hoechst+ cells co-label with PI. (h) Quantitation of PI+ cells in x200 fields between 1 h and 7 d after ICH. *$p < 0.05$ vs. 1 h, 7 d; **$p < 0.05$ vs. 1, 6, 24 h and 7 d. Scale bars: (a-e), 100 um; (f), 10 um; (g), 20 um.

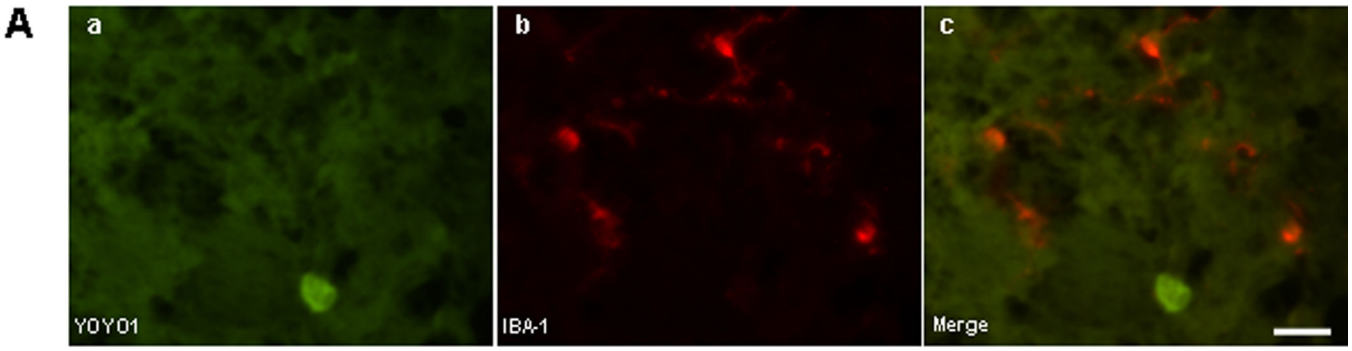

Figure 2a

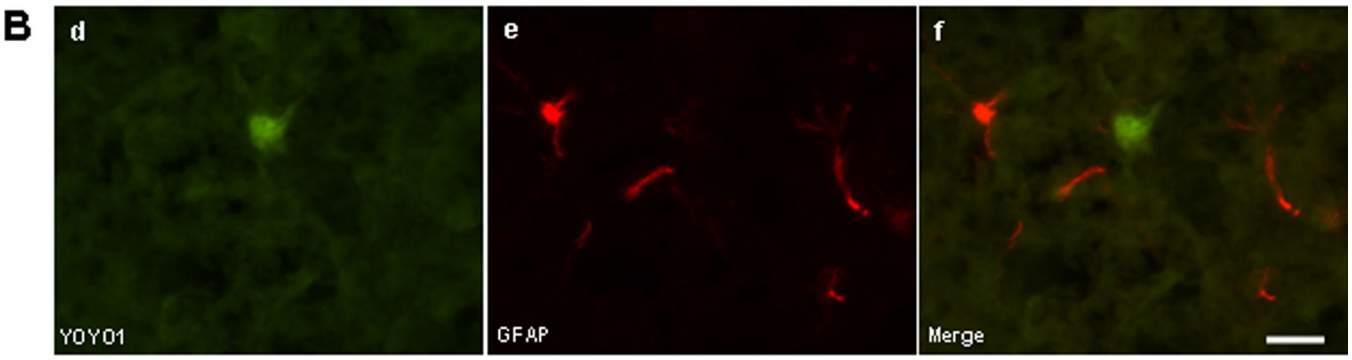

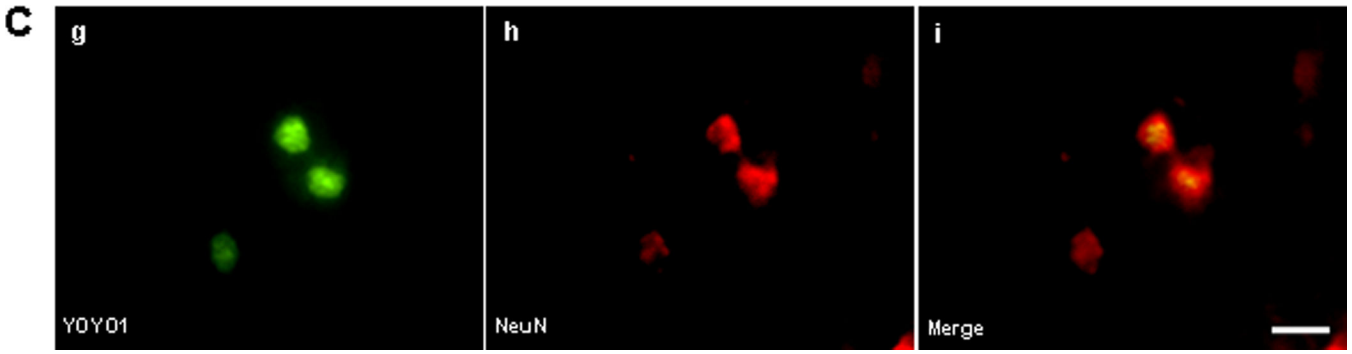

Figure 2b

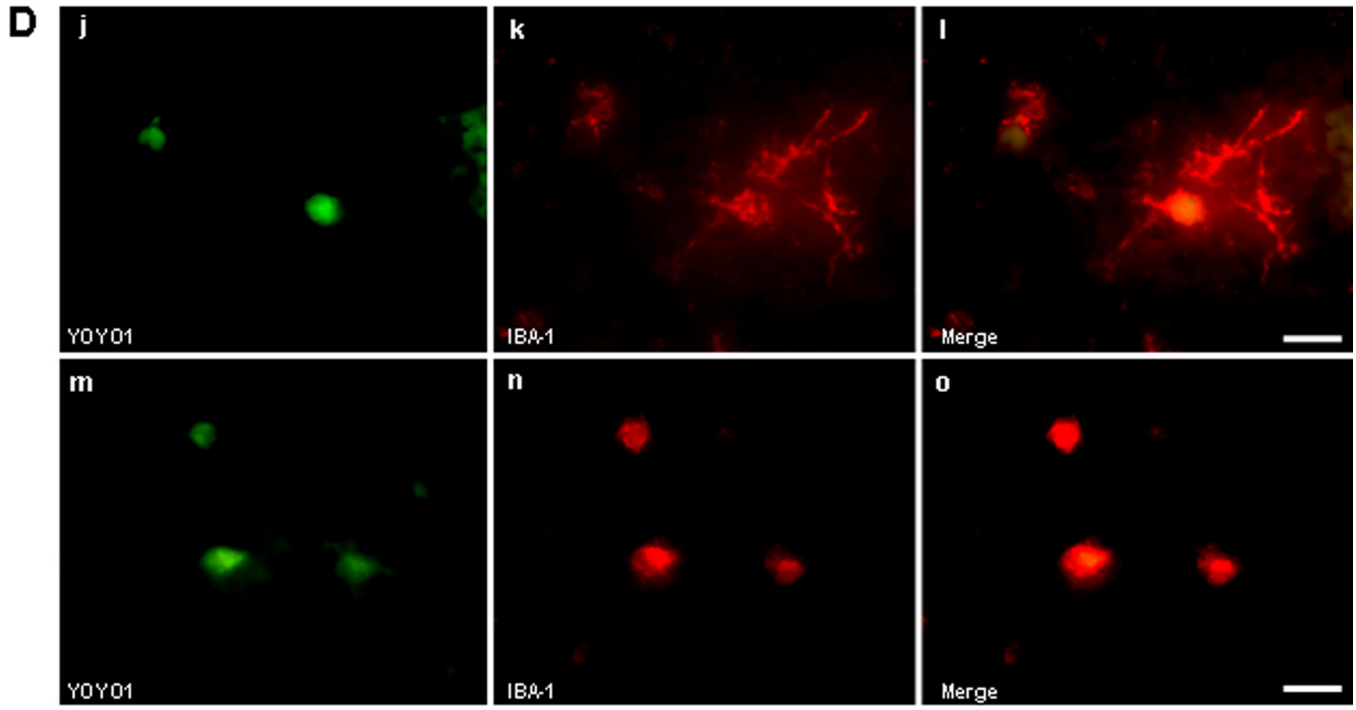

Figure 2d

Figure 2.

Identification of permeable cell types after intracerebral hemorrhage (ICH). (A-C) Detection of cell types with plasmalemma permeability to YOYO-1 iodide at 6 h after ICH. (A) Representative photomicrographs of YOYO-1+ cells (a), IBA-1+ (b), and overlay (c) showing no colocalization. (B) Representative photomicrographs of YOYO-1+ cells (d), GFAP+ cells (e), and overlay (f) showing no colocalization. (C) Representative photomicrographs of NeuN+ neurons (g) that colocalized with YOYO-1 (h) at 6 h after ICH (i, overlay) suggesting that neurons are particularly sensitive to plasmalemma damage early after ICH. (D) Detection of cell types with plasmalemma permeability to YOYO-1 at 24 h after ICH. By 24 h, YOYO-1+ cells (j) colocalized with IBA-1+ cells with morphological features of microglia (k) as shown in the overlay (l). YOYO-1+ cells (m) also colocalized with IBA-1+ cells with the morphological appearance of macrophages (n) at 24 h (o, overlay). Scale bar, 10 um for each panel.

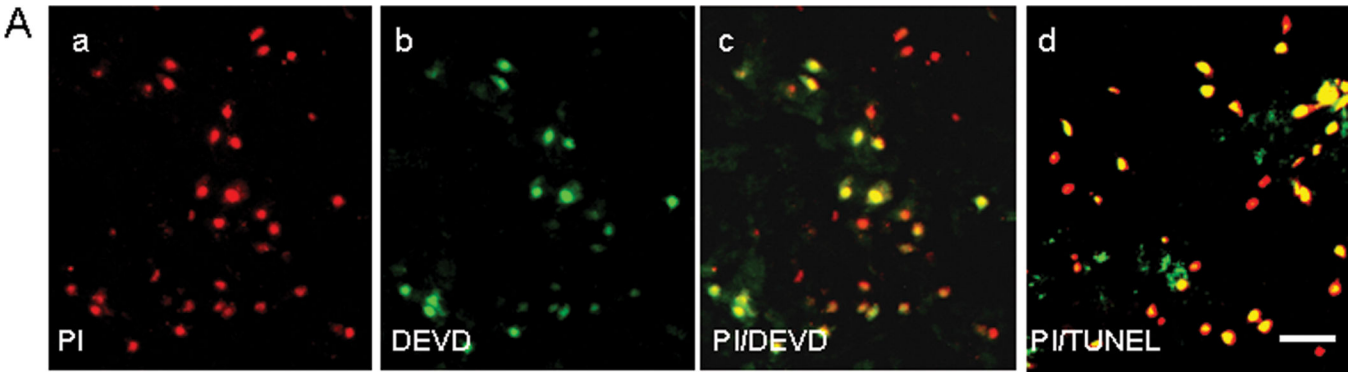

Figure 3a

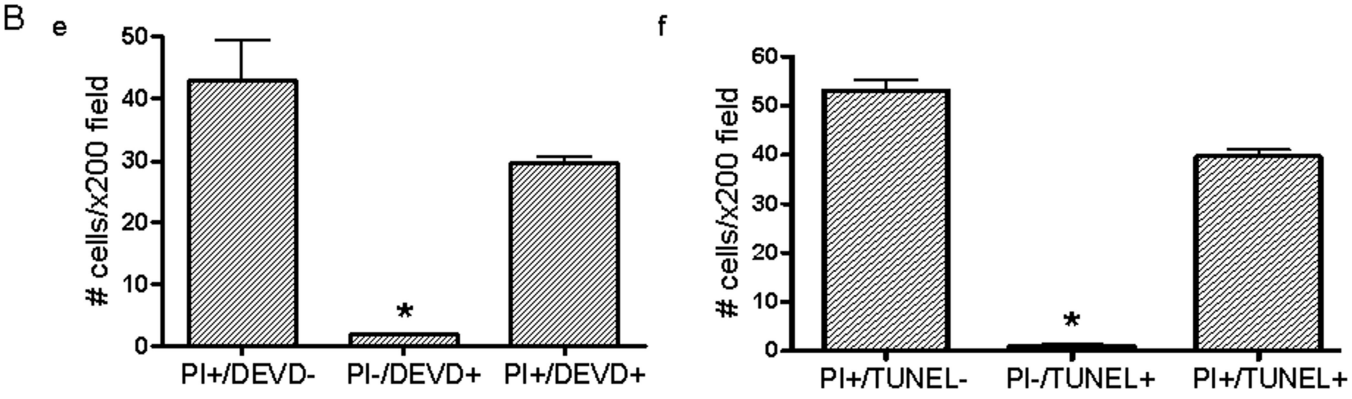

Figure 3b

Figure 3.

Association of cell death markers with PI+ cells after intracerebral hemorrhage. (A) Colocalization of caspase substrates and TUNEL with permeable cells 48 h after ICH. (a) In vivo PI stains permeable cells red. (b) DEVD labeling of the brain section in (a). (c) Overlay of a and b. (d) Overlay of a brain section labeled with in vivo PI (red) and ex vivo TUNEL (green). Only a few cells stained green and not red (PI−/TUNEL+). Scale bar, 40 um for each panel. (B) Quantitative analyses of PI+ cells labeled ex vivo with DEVD (e) or TUNEL (f) at 48 h after ICH. Values shown are averages of peripheral and core regions. *$p < 0.05$ vs. PI+/DEVD− and PI+/DEVD+ and PI+/TUNEL− and PI+/TUNEL+.

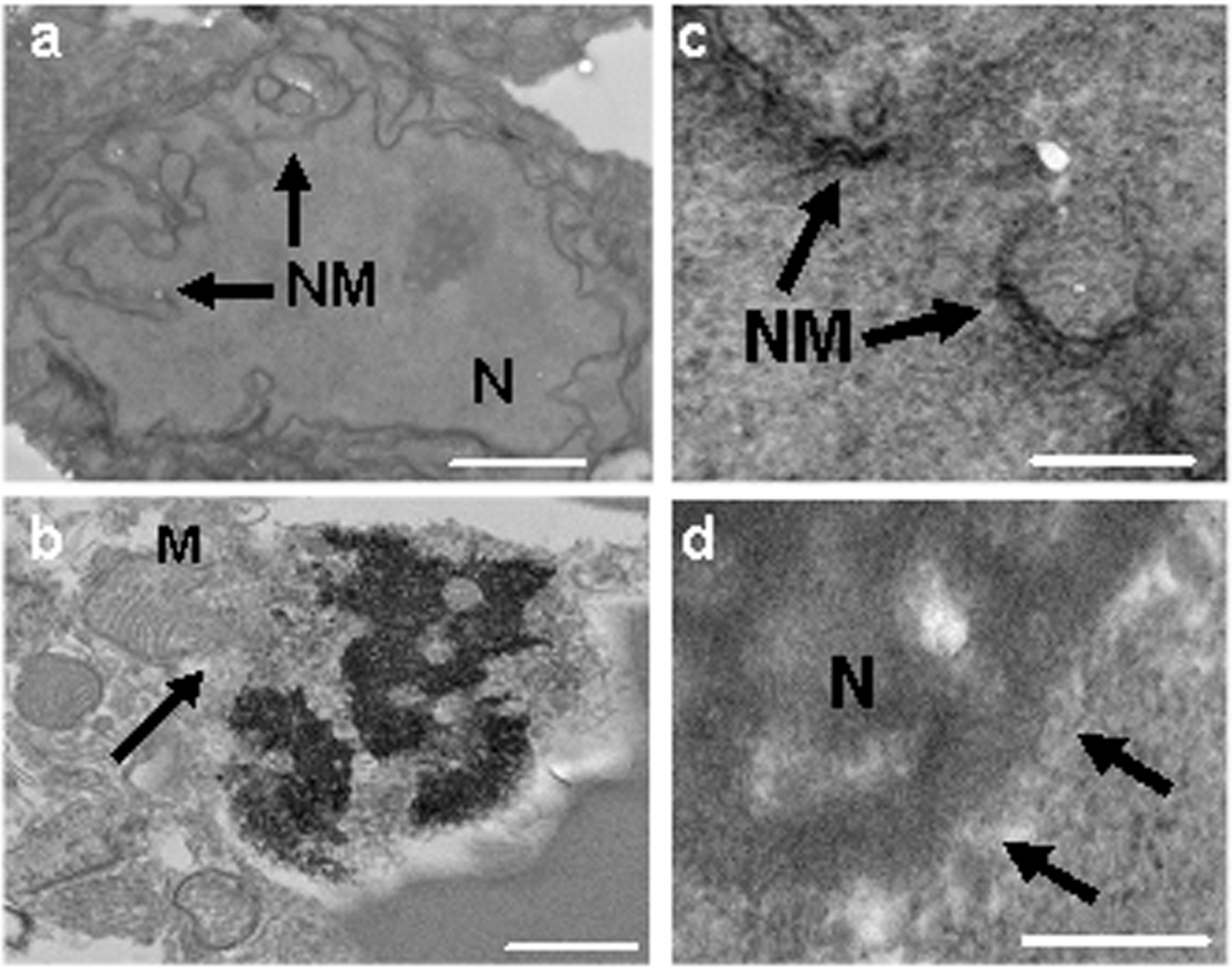

Figure 4.

Ultrastructural analyses of injured cells at 24 h after intracerebral hemorrhage. (a) Normal nucleus (N) and nuclear membrane (NM) of an intact neuron in the contralateral (uninjured) striatum showing intact cellular architecture. (b) Swollen mitochondria (M), nuclear karyorrhexis, and dissolution of the nuclear membrane with mitochondria entry into the nucleus in a cell with necrotic morphology. (c, d) Loss of nuclear membrane integrity consistent with necrosis (arrows indicate nuclear membrane). Scale bars: (a) 2 um, (b) 3 um, (c, d) 300 nm.

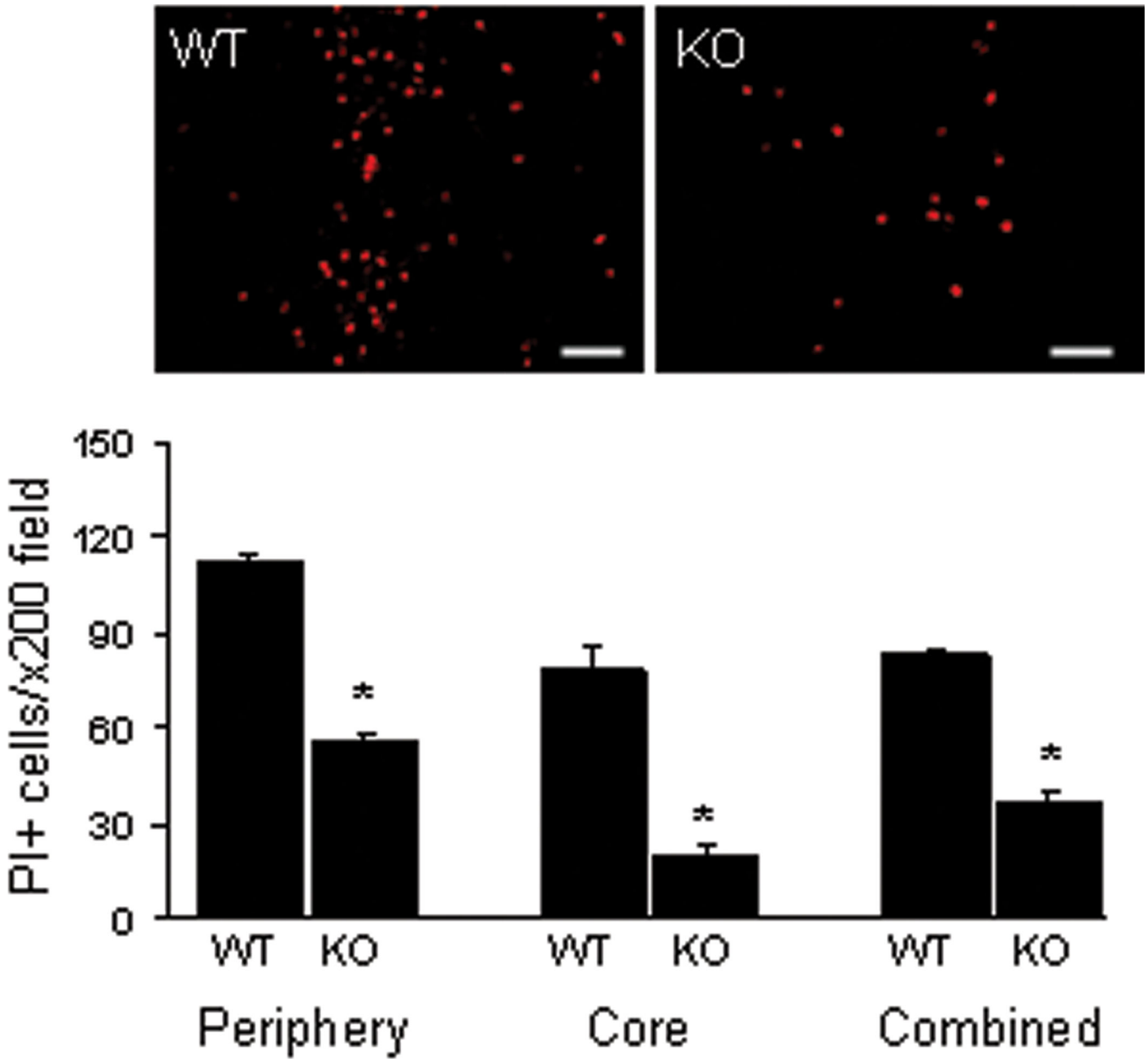

Figure 5.

Decreased PI+ cells at 24 h after intracerebral hemorrhage in mice deficient in receptor interacting protein kinase 3 (RIPK3 KO). Upper panels: Representative photomicrographs depicting PI+ cells in hemorrhagic brain 24 h after ICH in wild type (WT) and RIPK3 knockout (KO) mice. Lower panel: RIPK3 KO mice had significantly decreased PI+ cells in peripheral, core, and combined peripheral and core x200 fields at 24 h after ICH. *p = 0.008 vs. WT.

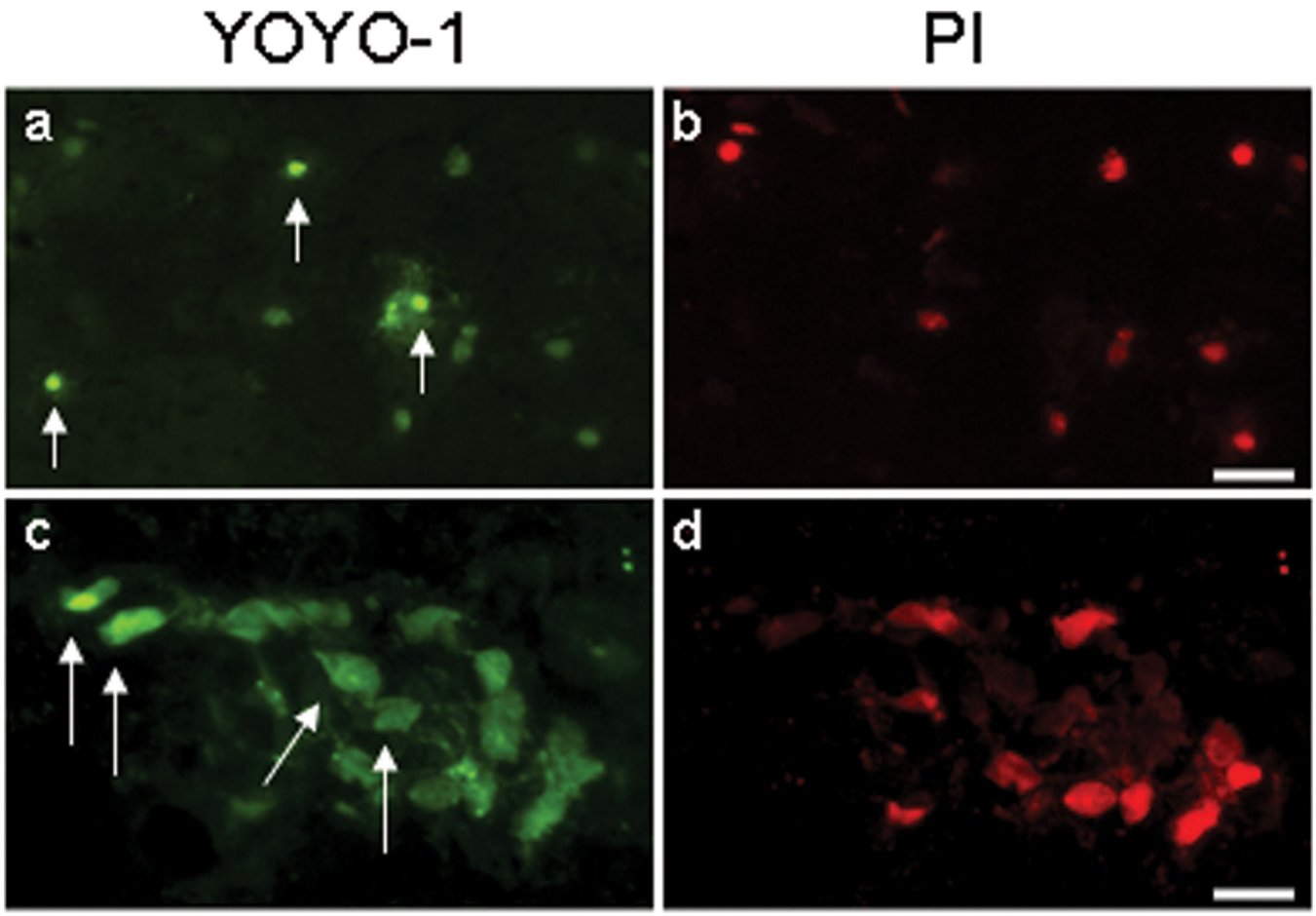

Figure 6.

Plasmalemma resealing after intracerebral hemorrhage. Mice were subjected to ICH and administered YOYO-1 at 24 or 48 h and PI at 48 or 72 h, respectively. (a–d) representative photomicrographs of brain sections showing YOYO-1+ and PI+ cells labeled at 24–48 h. Note that the majority of YOYO-1+ cells are also PI+, however some YOYO-1+ cells are PI-negative (arrows). Scale bars: (a, b) 60 um; (c, d), 20 um.